Arabian Journal of Chemistry (2023) **16**, 105042

King Saud University

Arabian Journal of Chemistry

www.ksu.edu.sa
www.sciencedirect.com

ORIGINAL ARTICLE

The feasibility study of CAU-1 as an adsorbent for Cu, Zn, Pb, As, Fe and endocrine disrupting chemical bisphenol-A (BPA)

Siti Nurfatin Nadhirah Mohd Makhtar [a,b], Mohamad Zahir Mohd Pauzi [a], Prakash Peechmani [a], Khairul Hamimah Abas [c], Mohd Hafiz Dzarfan Othman [a], Juhana Jaafar [a], Mukhlis A. Rahman [a,*]

[a] *Advanced Membrane Technology Research Centre (AMTEC), Universiti Teknologi Malaysia, 81310 Skudai, Johor, Malaysia*
[b] *Microelectronics and Nanotechnology-Shamsuddin Research Center, Institute for Integrated Engineering, Universiti Tun Hussein Onn Malaysia, 86400, Parit Raja, Batu Pahat, Johor, Malaysia*
[c] *Department of Control & Instrumentation Engineering, School of Electrical Engineering, Universiti Teknologi Malaysia, 81310 Skudai, Johor, Malaysia*

Received 29 August 2022; accepted 30 May 2023
Available online 5 June 2023

KEYWORDS

CAU-1;
Heavy metal removal;
BPA removal;
Chemisorption;
Spontaneous process

Abstract This work discusses the feasibility of CAU-1 as an adsorbent for both heavy metals and bisphenol A (BPA). CAU-1 was synthesised solvothermally at 120 °C for 8 h. Batch adsorption study was done to investigate the feasibility of CAU-1 as the adsorbent. The CAU-1 weight was constant throughout the study, 0.01 g. CAU-1 was characterised using zeta potential analysis, SEM, FTIR, TGA, and XRD. CAU-1 was only able to remove BPA and not able to adsorb heavy metals due to the repulsion forces between CAU-1 and the heavy metals. Thus, BPA was used as adsorbate for CAU-1 adsorption study. The optimum conditions for BPA adsorption on CAU-1 were at pH 7 and 3 h contact time. The adsorption capacity increased infinitely with increasing concentration of the BPA. The maximum equilibrium adsorption capacity (q_e) of CAU-1 for BPA was 310.1 mg/g at 25 °C, and the adsorption followed the pseudo-second-order kinetic model. The thermodynamic studies indicate that the adsorption reaction is a spontaneous and endothermic process, a favourable reaction.

* Corresponding author.
E-mail address: r-mukhlis@utm.my (M.A. Rahman).
Peer review under responsibility of King Saud University.

Production and hosting by Elsevier

https://doi.org/10.1016/j.arabjc.2023.105042
1878-5352

1. Introduction

Industrial wastewater commonly contains inorganic and organic substances, typically heavy metals and endocrine disrupting chemical (EDC). This issue has become a major concern globally (Srivastava and Majumder, 2008; Fu and Wang, 2011; Demirbas et al., 2006; Rani et al., 2020; Gonsioroski et al., 2020; Sun et al., 2020; Martín-Lara et al., 2020; Xu et al., 2012; Dehghani, 2016; Ahmed et al., 2017; Mpatani et al., 2021; Qasem et al., 2021; Chaiyasith et al., 2006; Alghamdi et al., 2019; Zhao et al., 2019; Hashem, 2007). Heavy metals are elements with atomic weights ranging from 63.5 to 200.6, with specific gravity values greater than 5.0 (Srivastava and Majumder, 2008). Heavy metal contamination has become a main concern due to its non-biodegradability, toxicity, carcinogenicity, and ability to accumulate in organisms (Fu and Wang, 2011; Demirbas et al., 2006). Lead, copper, mercury, chromium, zinc, cadmium, and nickel are the typical heavy metals found in the water reservoir, resulting from poor manufacturing waste management. The tolerance limit of lead (Pb), copper (Cu), zinc (Zn), and arsenic (As) are 0.01, 2.0, 5.0, and 0.01 mg/L, respectively, as stipulated by the World Health Organization (WHO). Exceeding the tolerance will cause severe damages to certain body parts such as liver, kidneys, and the immune system and may cause diseases such as anaemia (Rani et al., 2020). Thus, heavy metal contamination in water consumption sources should be terminated. Another emerging contaminant that has become worrisome is bisphenol A (BPA). It is often detected in water at the ppb level, the level for trace organic contaminants. BPA is hazardous as it can cause damage to the reproductive systems of humans and animals (Gonsioroski et al., 2020). Nowadays, BPA has been detected frequently in all types of water, i.e., wastewater, groundwater, surface water, and drinking water, due to the extensive production of epoxy resins, polycarbonate, and other plastics (Sun et al., 2020), as BPA is commonly used in the manufacturing of these materials (Martín-Lara et al., 2020; Xu et al., 2012; Dehghani, 2016).

Many technologies have been used to remove heavy metals, such as biological treatment, oxidation, chemical precipitation, ion exchange, reverse osmosis, membrane filtration, electrochemical treatment, photocatalytic degradation, phytoremediation, and adsorption (Ahmed et al., 2017; Mpatani et al., 2021). Among those technologies, adsorption is the most promising technique for heavy metals and BPA removal owing to its advantages such as low operating cost, high removal capacity, easy implementation, high efficiency, production of less by-product, and simple recovery process and fast regeneration treatment (Qasem et al., 2021; Chaiyasith et al., 2006; Alghamdi et al., 2019; Zhao et al., 2019; Hashem, 2007; Tsai, 2006). Hence, removing heavy metal and BPA contamination through adsorption is an enticing prospect for water purification. Various types of adsorbents have been investigated for heavy metal and BPA removal, including carbon-based adsorbents, chitosan-based adsorbents, mineral adsorbents, magnetic adsorbents, biosorbents, and metal–organic framework (MOF) adsorbents. Of all these adsorbents, MOF adsorbents have been utilised for heavy metals adsorption compared to other conventional adsorbents for the reason of having excellent absorption efficiency (Van De Voorde et al., 2014). MOFs that have been used in heavy metal removal include modified Universitetet i Oslo-66 (UIO-66) (Fu and Wang, 2011; Martín-Lara et al., 2020; Soltani et al., 2021; Boix, 2020), MOF-808 (Peng, 2018), modified zeolite imidazolate frameworks-8 (ZIF-8) (Huang, 2020), and bimetallic Fe–Mg MOF (Abo El-Yazeed et al., 2020).

MOF is a new material with an ordered structure that can be manipulated by combining metal ions and organic linkers. MOF is a three-dimensional organic–inorganic complex with highly porous nanostructures consisting of metal ions and organic linkers. MOF has exceptional advantages such as high surface area, tunable porosity and highly porous nanostructures, easy functionalisation, high exposure to chelating sites, various structures and topologies, high stability to chemical exposure, and controllable architecture (Xu et al., 2021; Qin et al., 2016; Allioux, 2018).

In this work, an aluminium-based MOF, named Christian-Albrecht-University (CAU-1) was chosen as an adsorbent to remove heavy metals and BPA, which are the most common pollutants nowadays. CAU-1 was built as pseudo-body octameric building blocks of aluminium ions and connected by aminoterephthalic ions, making the structure form of a tetragonal shape, $\{Al_8(OH)_4(OCH_3)_8\}12+$ (Zhao et al., 2019; Pauzi, 2019; Zheng et al., 2020; Kim et al., 2010; Zhong et al., 2021; Ahnfeldt et al., 2009). CAU-1 has gained much attention because it is a water-stable porous material, it possesses a rigid framework with exceptional thermal stability, and is easily synthesised with outstanding functional groups such as $–NH_2$ and –OH, which are ideal properties for adsorption (Zhong et al., 2021; Ahnfeldt et al., 2009; Zheng et al., 2020). The water-stable property resulted from the bond of aluminium atoms and methyl oxygen in CAU-1′s secondary structure unit. The bond hinders water molecules from attaching to CAU-1 (Kim et al., 2010). This facilitates the adsorption process by reducing the competition of water molecules and the adsorbate (Zhong et al., 2021). Regardless of these excellent properties, the application of CAU-1 as an adsorption material is limited. To the best of our knowledge, no study has been done on CAU-1 adsorption for heavy metals and BPA pollutant. Thus, in this study, CAU-1 was chosen as an adsorption material to investigate its feasibility to remove heavy metal ions and BPA from aqueous solutions in a batch adsorption system.

2. Experimental

2.1. Materials

Aluminium chloride hexahydrate ($AlCl_3{\cdot}6H_2O$), 2-aminoterephthalic acid ($H_2BDC–NH_2$), methanol (CH_3OH), and alumina (Al_2O_3), bisphenol A (BPA, $C_{15}H_{16}O_2$, Mw = 228.29 g/mol) were obtained from Merck, and used as is. Copper sulphate pentahydrate ($CuSO_4{\cdot}5H_2O$, 98% purity, Mw = 159.61 g/mol), zinc sulphate heptahydrate ($ZnSO_4{\cdot}7H_2O$, Mw = 287.54 g/mol), lead (II) nitrate ($Pb(NO_3)_2$, Mw = 33 1.2 g/mol), arsenic trioxide (As_2O_3, Mw = 197.84 g/mol), and iron(II) sulfate (Fe_2SO_4, Mw = 151.91 g/mol) were purchased from Sigma-Aldrich.

2.2. Synthesis of CAU-1

CAU-1 was produced through solvothermal technique. $AlCl_3{\cdot}6H_2O$ (12.3 mmol) and $H_2BDC–NH_2$ (4.1 mmol) were mixed with CH_3OH (30 mL) for 30 min. The mixture was then poured into a Teflon-lined autoclave and heated at 120 °C for 8 h. The mixture was cooled and then rinsed with CH_3OH thrice. Distilled water was used for the final step of the rinsing process. The product was dried in a vacuum oven at 100 °C for 8 h (Ahnfeldt, 2009).

2.3. Characterisation

The samples were characterised by X-ray diffraction (XRD), scanning electron microscopy (SEM), nitrogen adsorption–desorption isotherms, Fourier transform infrared spectroscopy (FTIR), thermogravimetric analysis (TGA), and zeta potential analysis. XRD analysis was performed using Philips PW1710 at a scan rate of 1°/s, ranging from 4° to 22°. SEM analysis was performed by using TM 3000, Hitachi. The samples were coated with platinum under vacuum for 1 min at 20 mA. Nitrogen adsorption–desorption isotherms were obtained using BET characterisation (Micromeritics TriStar II). The sam-

ples were degassed for 5 h at 120 °C under vacuum prior to the measurement. FTIR analysis was performed using Nicolet iS10 (Thermo Scientific) with the KBr method. The spectrum was recorded at wavelengths ranging from 500 to 4000 cm^{-1}. The scanning repetition process was fixed at 32 times. The thermal stability of CAU-1 was determined using TGA Q500, Thermo Fisher under air, from 30 to 750 °C with a heating rate of 5 °C/min. Surface charge was measured in ultrapure water using a zetameter (Malvern Zetasizer Nano ZSP) at pH 7.

2.4. Batch adsorption studies

The adsorption studies were conducted via batch mode containing 50 mL of relevant solutions, i.e., heavy metal (lead, arsenic, iron, zinc, and copper) and BPA solutions. The CAU-1 adsorbent was fixed at 0.01 g for all the adsorption studies. The mixture was agitated at 150 rpm in a temperature-controlled water bath (Grant TX150, United Kingdom). Optimum parameters for adsorption such as pH, contact time, and initial concentration of the adsorbate were studied to obtain the highest removal efficiency of pollutants by CAU-1. The desired pH of the adsorbate solution was maintained using suitable buffer solutions, namely HCl and NaOH. The heavy metal concentrations were determined using atomic absorption spectroscopy (AAS), Shimadzu AA-7000, Japan. A calibration curve of absorbance versus concentration was plotted for each heavy metal tested to calculate the removal efficiency (%) and adsorption capacity (q_e) using Eqs. (1) and (2), respectively.

$$Removalefficiency(\%) = \frac{C_0 - C_t}{C_0} \times 100\% \quad (1)$$

$$Adsorptioncapacity(\frac{mg}{g}) = \frac{V}{m}(C_0 - C_t) \quad (2)$$

where C_0 is the initial concentration (mg/L), C_t is the concentration after time t in the solution (mg/L), V is the initial volume of the sample (L), and m is the mass of CAU-1 (g).

2.5. Adsorption kinetics

The adsorption kinetics data were used to determine the mechanism of the adsorption process and the relationship between the adsorption time and adsorption capacity through the fitted kinetic model. The equations involved for the kinetic model's investigation are Eqs. (3), (4), and (5) for pseudo-first-order, pseudo-second-order, and intraparticle diffusion, respectively (Yusuff et al., 2019).

$$\log(q_e - q_t) = \log q_e - k_1 t \quad (3)$$

where q_e is the theoretical equilibrium adsorption capacity (mg/g), q_t is adsorption capacity (mg/g), k_1 (min^{-1}) is the pseudo-first-order constant, and t (min) represents the time of adsorbate adsorption to occur. A graph of log ($q_e - q_t$) against t was plotted to calculate the value of q_e and k_1 from the intercept and slope, respectively.

$$\frac{t}{q_t} = \left(\frac{1}{q_e}\right)t + \frac{1}{k_2 q_e^2} \quad (4)$$

where t (min) represents the time of adsorbate adsorption to occur, k_2 is the pseudo-second-order constant (g/mg•min), q_t is the amount of adsorbate adsorbed at time t (mg/g), and q_e is the amount of adsorbate adsorbed at equilibrium (mg/g). A graph of t/q_t versus t was plotted to determine the values of q_e and k_2 from the slope and intercept, respectively.

$$q = k_{ip} t^{1/2} + C_i \quad (5)$$

where q is the amount of adsorbate adsorbed at time t (min), k_{ip} is the intraparticle diffusion rate constant (mg/g•$min^{1/2}$), and C_i is the intercept.

2.6. Adsorption isotherms

The isotherm models were investigated to study the correlation of the adsorbate adsorbed onto CAU-1 and the adsorbate equilibrium concentration in the solution. The adsorption isotherm was studied using Langmuir and Freundlich isotherm models. The Langmuir isotherm model shows monolayer adsorption if the adsorbates adsorb on homogeneous active sites until saturation is achieved, which is a state where no further adsorption occurs. Langmuir isotherm model also reveals no interaction between the adsorbed molecules on adjacent sites (Yusuff et al., 2019). Meanwhile, the Freundlich isotherm discloses multilayer adsorption on a heterogeneous surface. The linear forms of Langmuir and Freundlich models are expressed in Table 1.

2.7. Adsorption thermodynamic

The thermodynamics calculation for Gibbs free energy (ΔG), enthalpy (ΔH), and entropy (ΔS) were performed using Van 't Hoff equation as shown in Eqs. (8) and (9) (Lazim, 2021; de Farias et al., 2021; Li et al., 2021).

$$\Delta G = -RTInK \quad (8)$$

$$InK = -\frac{\Delta H}{RT} + \frac{\Delta S}{R} \quad (9)$$

where K is the equilibrium constant, R is the gas constant (8.314 J/mol•K), T is the temperature (K), ΔG is the Gibbs free energy changes (kJ/mol), ΔH is the enthalpy changes (J/mol), and ΔS is the entropy changes (J/mol.K).

3. Results and discussion

3.1. Physical and chemical characteristics of CAU-1

CAU-1 characteristics were analysed using zeta potential analysis, SEM, BET, FTIR, TGA, and XRD. CAU-1 surface charge was identified using zeta potential analysis at pH 7. At neutral condition, CAU-1 has a positive charge, with a value of 17.7 mV. The morphology and particle size of CAU-1 were studied using SEM as shown in Fig. 1. CAU-1 shows significant crystal grains, an indicator of typical crystalline materials. CAU-1 has a rice shape as reported by Zhao et al. (Zhao et al., 2019) with a smooth surface and particle size of ≈2.11 μm.

N_2 adsorption–desorption analysis was performed to characterise the microporosity in the synthesised CAU-1 using N_2

Table 1 Langmuir and Freundlich isotherm models in linear form.

Model	Equation	Remarks	Equation
Langmuir	$\frac{C_e}{q_e} = \left(\frac{1}{q_m}\right)C_e + \frac{1}{q_m K_l}$	C_e is the concentration at equilibrium (mg/L)Q_e is adsorbed quantity at equilibrium (mg/g) Q_m is the adsorption efficiency constantK_l is the adsorption energy constant	6
Freundlich	$\log q_e = \log K_f + \frac{1}{n} log C_e$	Q_e is the amount of adsorbate adsorbed (mg/g)C_e is the concentration of adsorbate in solution at equilibrium (mg/L)K_f and n are the constants integrating all factors affecting the adsorption capability and adsorption intensity, respectively	7

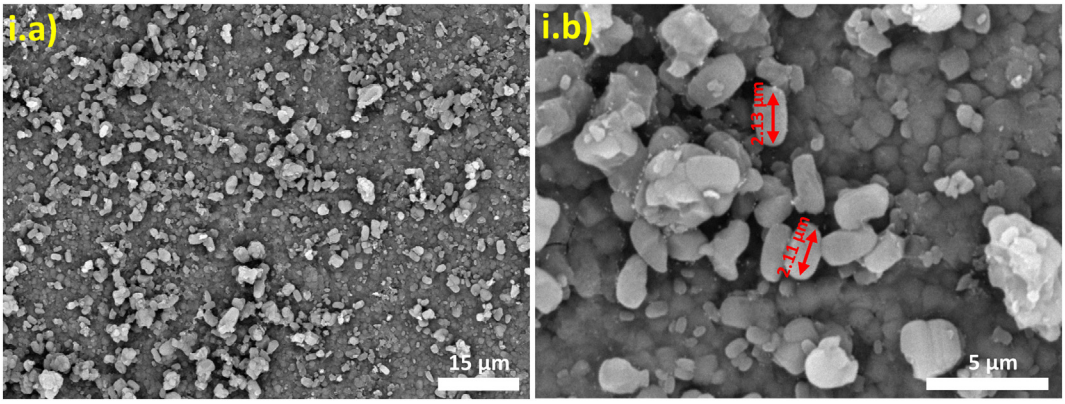

Fig. 1 Surface morphology of CAU-1 at i.a) 2 k magnification and i.b) 9 k magnification.

isotherms as shown in Fig. 2(i). Fig. 2(i) reveals the potential of CAU-1 as an adsorbent. The CAU-1 adsorbed a significant amount of N_2, indicating the presence of micropores in the CAU-1 structure. Fig. 2(i) also shows a hysteresis loop at P/P_0 from 0.4 to 0.9, denoting that the pores are nearly vertical, which indicates a very narrow distribution of pore sizes. Agglomeration was found in the CAU-1, represented by the significant N_2 adsorption at $P/P_0 > 0.9$ in the figure. The BET specific area of CAU-1 was calculated to be 1037.6155 $m^2 \cdot g^{-1}$ from the N_2 adsorption and desorption isotherms at 77 K, which is similar to the reported value of 1249 $m^2 \cdot g^{-1}$ (Zhao et al., 2019). This is due to the particle size of the CAU-1 itself. Smaller particles have higher surface area while bigger particles have less surface area.

Fourier transform infrared spectroscopy (FTIR) analyses were carried out to study the functional groups in CAU-1 for the adsorption process. Fig. 2(ii) depicts the FTIR spectra for the synthesised CAU-1. Several characteristic peaks of CAU-1 appeared at 3326, 1625, 1425, 1107, 1238, and 754 cm^{-1}. A primary asymmetric amine group (N–H) was observed at 3326 cm^{-1}, with the signature spike of amine at 3162 cm^{-1}. The shoulder band of primary amine is also present in the spectrum, confirming the existence of the primary amine. Aminoterephthalic acid, a ligand in the CAU-1, was detected through the C═O functional group at 1625 and 1425 cm^{-1}. C—O and C—N bonds correspond to peaks at 1107 and 1238 cm^{-1}, respectively. Al—O—Al was observed at 754 cm^{-1}, indicating that the CAU-1 framework is connected through the bonding of aluminium and oxygen (Zhong et al., 2021). It can be concluded that the synthesised CAU-1 framework was constructed via C—O, C—N, C═O, and Al—O—Al bonds.

The TGA curve of CAU-1 was depicted as a three-stage weight loss as shown in Fig. 2(iii). The weight loss in the first stage was due to the dehydration process. The hydration process occurred at 30 to 100 °C. The second stage of weight loss at 200 °C was ascribed to the CAU-1′s framework collapse, which denotes the optimum CAU-1 framework stability towards temperature. The third stage of weight loss at 546 °C was attributed to the further CAU-1 framework collapse owing to the destruction of $H_2BDC–NH_2$ in the framework (Zhong et al., 2021).

The crystal growth of CAU-1 orientation was examined by X-ray diffraction as shown in Fig. 2(iv). The notable peaks of CAU-1 are seen at 6.9°, 9.9°, 13.8°, and 19.9°, with the lattice planes (011), (002), (022), and (001), respectively. The observed plane in the XRD shows that the CAU-1 crystal orientation was built by coordination sites of inorganic building blocks. Lattice planes (002) and (001) revealed that the CAU-1 crystals are attached to the functional interface during the growth. The peak at 9.9° in the spectrum indicates the CAU-1 crystals attached to the –OH terminal interface at plane (002), whereas the peak at 19.9° implies that the CAU-1 crystals attached to —COOH functional interface at plane (001) (Gölzhäuser, 2010). Plane (011) exists when the aluminium ions in CAU-1 as the coordination sites are constructed as a wheel-shaped block. Based on Florian et al., (Gölzhäuser, 2010) the CAU-1 crystals have their own preferred growth orientation, which can be distinguished based on the lattice plane and shape of the crystals. CAU-1 crystal growth oriented by (011) plane would have tetragonally shaped crystals (like a rice shape) while (002) plane would have a cubic shape. The shape can be observed and validated by SEM images. Thus, in this study, CAU-1 crystals domi-

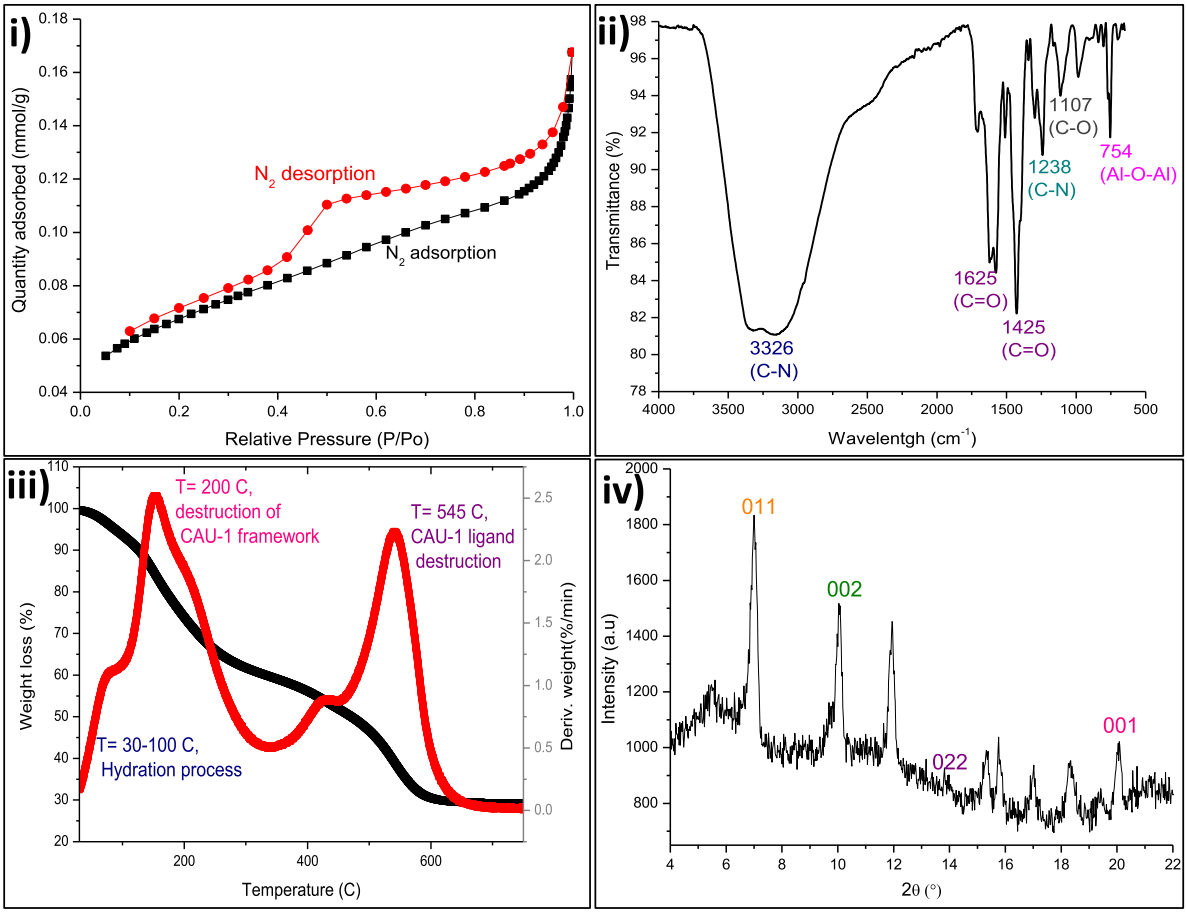

Fig. 2 Characteristics of CAU-1. (i) N_2 adsorption–desorption isotherms of CAU-1 crystals, (ii) ex situ infrared spectra of CAU-1 crystals, (iii) thermal stability of CAU-1 and thermogravimetric weight loss of CAU-1 heated in air, and (iv) XRD orientation of CAU-1 lattice planes.

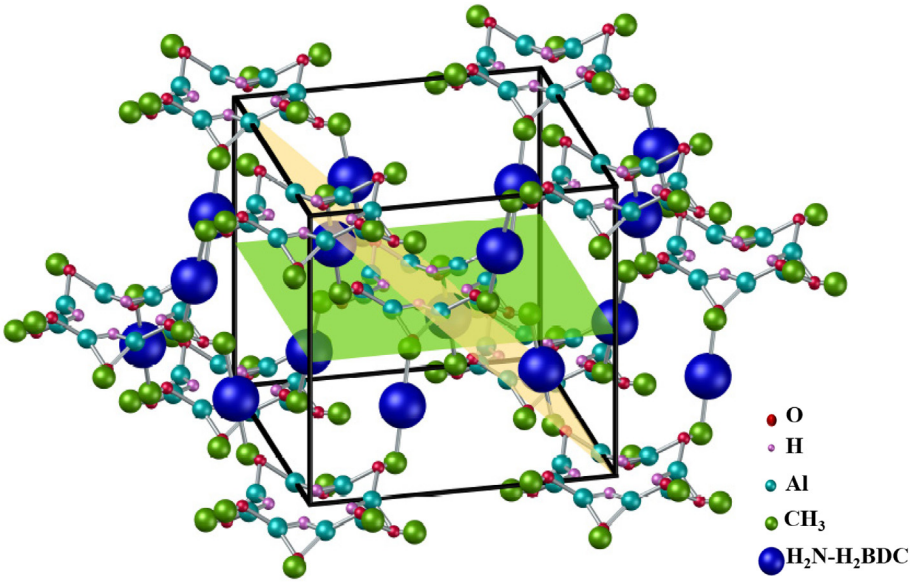

Fig. 3 Schematic structure of CAU-1 crystal, with (011) plane. yellow and (002) plane. green.

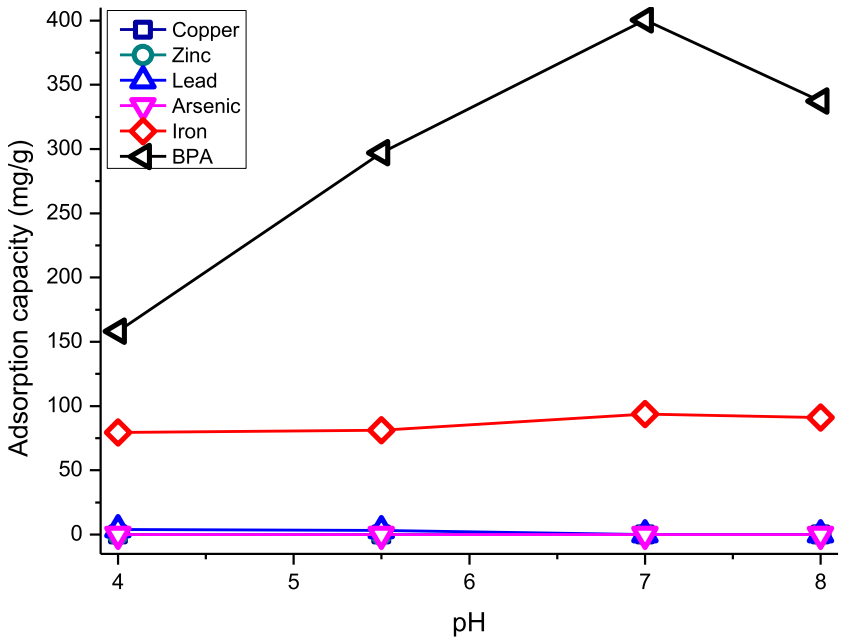

Fig. 4 CAU-1 adsorption capacity copper, zinc, lead, arsenic, iron, and BPA.

nantly grow by the (0 1 1) planar direction even though both planes can be observed in the XRD spectrum, as proven by the SEM images in Fig. 1. The schematic structure and plane of CAU-1 crystals are illustrated in Fig. 3. The structure was drawn based on CCDS database 723320, skeletal structure (Pauzi, 2019), and planar orientation (Gölzhäuser, 2010).

3.2. Adsorption studies of CAU-1 towards heavy metals and BPA

CAU-1 adsorptions were tested on heavy metals and bisphenol A (BPA) as shown in Fig. 4. The adsorption for heavy metal was done at pH 4.0, 5.5, 7.0, and 8.0 to observe the capacity at acidic, neutral, and basic conditions for metal ions aluminium (Al), copper (Cu), zirconium (Zr), zinc (Zn), lead (Pb), iron (Fe) and arsenic (As). CAU-1 could only adsorb iron in basic and acidic mediums, preferably in basic medium (pH 8). This can be attributed to the attraction of CAU-1′s positive surface charges with the metal at basic condition. The OH ions help to reduce the repulsion forces between the CAU-1′s positive surface charges and positive metal ions. However, this phenomenon is only applicable to iron, as shown in Fig. 4. This is due to the peculiar properties of iron metal, which precipitates in acidic condition. Other metal ions such as Cu, Zn,

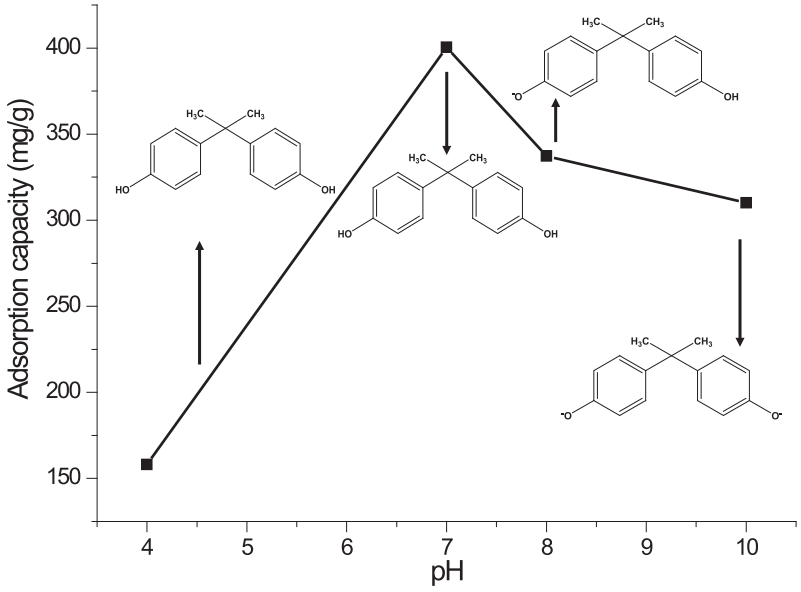

Fig. 5 Adsorption capacity of CAU-1 for 100 ppm BPA at room temperature for 3 h.

Pb, and As precipitate in basic condition, which is unfavourable in the CAU-1 adsorption. Thus, CAU-1 was not suitable to be used as an adsorbent for metals that precipitate in basic condition. Bisphenol A (BPA) was also tested for CAU-1 adsorption. CAU-1 was able to adsorb BPA with the rejection of 48.25% at 30 min, using 0.01 g CAU-1. It can be concluded that CAU-1 is suitable for the adsorption of anionic and neutral compounds. Hence, BPA batch adsorption was further investigated.

3.3. BPA removal study using CAU-1

3.3.1. Effect of pH

pH is one of the vital parameters in adsorption studies, as it affects the electrical surface charge of the CAU-1 and the dissociation constant (pK_a) of the BPA. BPA adsorption is greatly related to the charge density of the CAU-1 and the charge of the BPA species in the selected media, either acidic or alkaline medium. A range of pH, from 4.0 to 10.0, was studied as shown in Fig. 5. The pKa value of BPA is 9.3, which indicates that the BPA exists as molecules before the first protonation at pH 8 (the BPA starts to lose hydrogen ion to the media) and continues to deprotonate at pK_a greater than 9.3. Based on Fig. 5, the maximum adsorption capacity is at pH 7, followed by pH 8, pH 10, and pH 4. In a study by Farias et al. (de Farias et al., 2021), BPA is reported as neutral, with zero surface density charge at pH 5–7. The adsorption capacity was greatly decreased in an acidic medium. This is due to the repulsive forces between the CAU-1 and BPA surface charge density. BPA surface density charge at pH 4 is positive and CAU-1 surface density charge is also positive, thus escalating the electrostatic repulsion and limiting the adsorption efficiency process as shown in Fig. 5. The adsorption capacity decreased slightly at pH 8 and 10. However, the main reason behind this was not the electrostatic repulsion forces but the interaction of BPA and CAU-1 functional groups itself (Cristina, 2019).

3.3.2. Effect of contact time

Another vital parameter in the batch adsorption study is contact time. The effect of contact time was investigated from 1 to 8 h, while other parameters were kept constant: 0.01 g CAU-1, pH 7, and 250 rpm shaking speed. Fig. 6 reveals that the adsorption capacity increased from 1 to 3 h, and began to achieve equilibrium at 4 to 8 h. The highest adsorption capacity was observed at 3 h, with the value 400.4 mg/g and 80% rejection. The adsorption capacity increased up until 3 h due to the availability of active sites at the initial stage of adsorption (Harja et al., 2022). The adsorption capacity decreased from 400.4 to 310.1 mg/g and from 80% rejection to 75% rejection at 4 h. This is attributed to the small number of active sites available for the BPA adsorption (Yap and Priyaa, 2019). The adsorption capacity and % rejection of BPA remained constant starting at 4 h and remained constant up until 8 h. The adsorption capacity was predicted to remain constant even if the contact time is prolonged due to the equilibrium uptake of BPA by CAU-1. An equilibrium uptake is defined as the time when the amount of BPA adsorbed on the CAU-1 and the amount of BPA in solution no longer change with time (Aragaw and Alene, 2022). In this study, 4 h is the starting point of the equilibrium state of BPA adsorbed on the CAU-1. Thus, 4 h was chosen as the optimised condition to study the effect of initial BPA concentration.

3.3.3. Effect of initial BPA concentration

The effect of initial BPA concentration ranging from 20 to 300 ppm was investigated using 0.01 g CAU-1 at pH 7. The effects of initial BPA concentration can be observed from the CAU-1 adsorption capacity and BPA removal percentage. The adsorption capacity of CAU-1 is correlated to the initial BPA concentration as shown in Fig. 7. The adsorption capacity of 20 and 300 ppm BPA increased from 79.99 to 722.53 mg/g, respectively. The adsorption capacity increased infinitely with the increasing BPA concentration; such a trend is com-

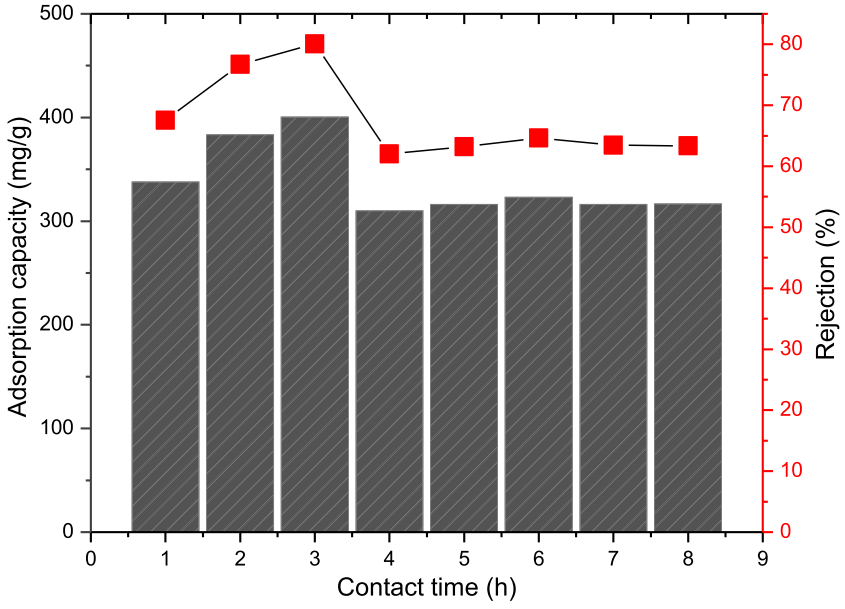

Fig. 6 Effect of contact time on the removal of BPA (adsorption capacity and rejection) using 0.01 g CAU-1 at pH 7 and 250 rpm shaking speed.

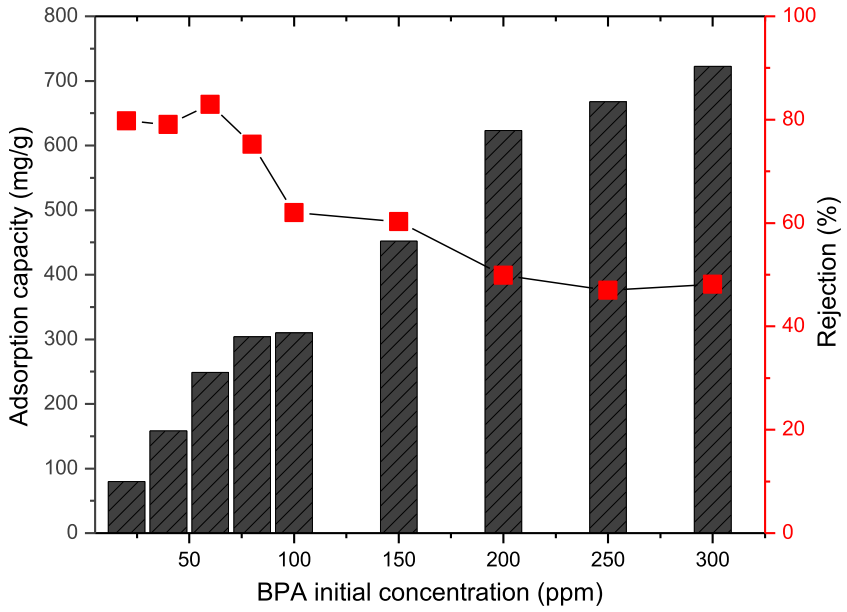

Fig. 7 Effects of initial BPA concentration ranging from 20 to 300 ppm on 0.01 g CAU-1 adsorption performance via adsorption capacity and rejection at pH 7.

Table 2 Kinetic model parameters of pseudo-first-order, pseudo-second-order, and intraparticle diffusion for BPA adsorption.

Kinetic model	Parameters		
Pseudo-first-order	K_1 (min^{-1})	q_e (mg/g)	R^2
	0.2315	19.169	0.6005
Pseudo-second-order	K_2 (g/mg.min)	q_e (mg/g)	R^2
	0.0121	303.03	0.9937
Intraparticle diffusion	K_p (g/mg•$min^{0.5}$)	C	R^2
	37.371	414.66	0.4697

Table 3 Isotherm model parameters of Langmuir and Freundlich for experimental BPA data.

Isotherm model	Parameters		
Langmuir	q_m (mg•g^{-1})0.0014153	k_L (L•mg^{-1})9.29	$R^2$0.6385
Freundlich	k_F (L•g^{-1})8.0501	1/n0.806	$R^2$0.9804

mon in Freundlich isotherm, confirmed by Table 3 in Section 3.5. This was attributed to the non-uniform adsorption nature of the CAU-1 itself (Deng et al., 2018). In addition, the increasing adsorption capacity was also due to the increasing driving force needed to overcome the mass transfer resistance between aqueous and solid phases (Fuzil, 2021).

Fig. 7 depicts that the BPA removal percentage decreased with increasing initial concentration. This was attributed to the less availability of active sites on the CAU-1 surface to adsorb BPA. The highest rejection percentage of 83% was achieved at 60 ppm initial BPA concentration. At this adsorption stage, the BPA quantity that needs to be adsorbed is less than the available active sites. However, as the BPA was increased, the available active sites became less accessible and insufficient. This is when CAU-1 was saturated, and no further adsorption occurred. Thus, the removal efficiency of BPA by CAU-1 decreased.

3.4. Adsorption kinetics study

Kinetics study is used to determine the removal rate of BPA from the aqueous solution. The adsorption mechanism and rate-controlling step were explored using three models, which are pseudo-first-order, pseudo-second-order, and intraparticle diffusion models. In this work, the experimental data to determine the adsorption kinetics for BPA adsorption were obtained by immersing 0.01 g CAU-1 into a solution with 100 ppm BPA for 60 to 480 min. Eqs. (3), (4), and (5) were used to determine the BPA adsorption kinetics.

Table 2 lists the kinetic parameters of pseudo-first-order, pseudo-second-order, and intraparticle diffusion for BPA adsorption. The highest fitted correlation coefficient (R^2) was obtained for the pseudo-second-order kinetic model with a value of 0.9937, indicating that the BPA adsorption mechanism onto CAU-1 is either chemisorption or electrostatic attraction

(Zhong et al., 2021). The reaction depends on the amount of solute adsorbed on the adsorbent surface and the amount adsorbed at equilibrium (Fuzil, 2021). In fact, the adsorption capacity (q_e) values attained from the model and the experiment were close, which are 303.03 and 310.10 mg/g, respectively.

Chemisorption is the transfer, exchange, or sharing of valence electrons between adsorbates and adsorbents. Chemisorption also implies that the adsorption process occurs via a chemical interaction between BPA and CAU-1, forming a chemical bond between them (Deng et al., 2018; Lalley et al., 2016; Petit, 2018). Thus, from the experimental kinetics study, the pseudo-second-order model suggests that CAU-1 and BPA formed a new chemical bond, either ionic or covalent, on the unsaturated metallic sites or on the CAU-1 functional groups, which is consistent with the FTIR spectrum after the adsorption as shown in Fig. 8. The FTIR spectrum in Fig. 8 illustrates a slight change in the functional groups. A carbonyl group (C = O) peak at 1636 cm^{-1} from the ligand disappeared after the BPA adsorption, without any new peak formation, confirming the chemisorption nature of the adsorption process.

3.5. Isotherm adsorption study

Isotherm adsorption was examined at pH 6.8 with 0.01 g CAU-1 for BPA concentrations from 20 to 300 ppm. The isotherm models for the BPA study were fitted using Langmuir and Freundlich models. The adsorption isotherm shows the relationship of the adsorbed sorbate quantity over adsorbent to the equilibrium solute concentration at a constant temperature (Rajahmundry et al., 2021). The values in Table 3 were obtained by plotting a graph using the equations provided in Table 1. Based on the R^2 coefficients, the BPA isotherm fits well with the Freundlich model, as shown in Table 3. The Freundlich adsorption isotherm reveals that BPA molecules adsorbed onto CAU-1 in a multilayer form, and the adsorption occurred through the chemical interaction of the CAU-1 and BPA. This is confirmed by the adsorption capacity (n) value from the Freundlich parameter. The n value is greater than 1, implying that the adsorption is a chemical interaction, consistent with the kinetic data in Section 3.4. The adsorption capacity (n) is the extent of the non-linearity between the solution concentration and the adsorption process. If n is greater than 1, the adsorption occurs through a chemical process. If n is < 0, the adsorption occurs through a physical process. If n is equal to 1, the adsorption process is not favourable by the adsorbate itself (Muhamad, 2018). In addition, the adsorption takes place in a non-uniform distribution, thus the adsorbed BPA molecule increases infinitely with increasing concentration, as proven in Fig. 9 (Deng et al., 2018). Fig. 9 illustrates the chemisorption process of BPA on CAU-1, based on the pseudo-second-order kinetic model and isotherm model as reported in Table 2 and Table 3, respectively. A comparison of kinetic and adsorption isotherms from various works is listed in Table 4. It was found that the adsorption isotherm for BPA followed Langmuir model for most adsorbents, however Freundlich model was obtained for CAU-1 used in this work. This may be attributed to the CAU-1 properties itself, that prefer the multilayer adsorption due to the forces available in the CAU-1 lone pairs, which can cause interaction to occur. A report on the CAU-1 interaction due to lone pair attraction have been reported by Pauzi et al., (Pauzi, 2019).

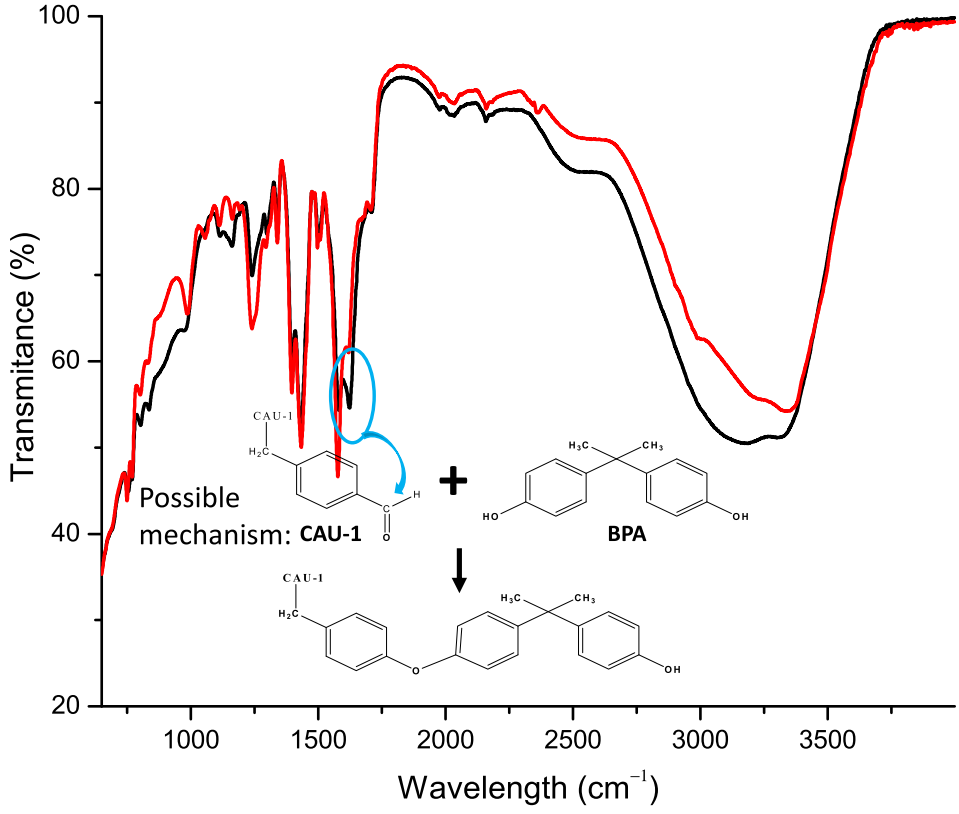

Fig. 8 FTIR spectrum of bare CAU-1 (—) and CAU-1 after BPA adsorption (—) for 4 h at pH 7.

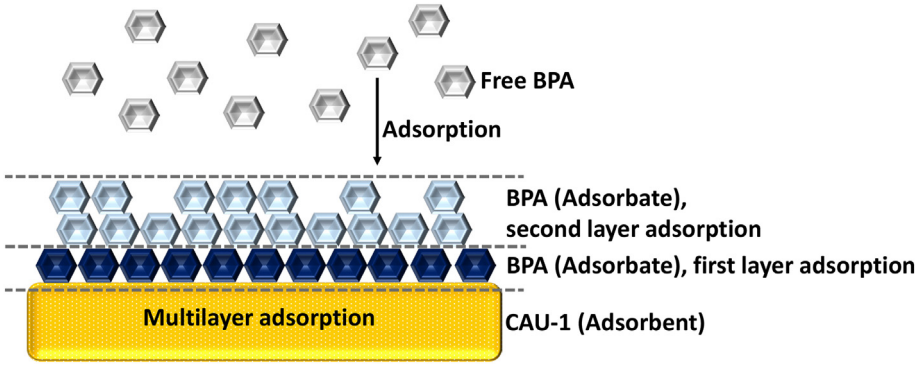

Fig. 9 Illustration of BPA adsorption process on CAU-1, a chemisorption with multilayer adsorption.

Table 4 Comparison of various adsorbents from previous studies.

Adsorbent	Kinetic study	Adsorption isotherm	Adsorption parameter	References
Graphene	Pseudo-second-orderq_e = 90.74 mg/gk_2 = 0.033 g/mg•min	Langmuirk_l = 0.5435 L/mg	Initial concentration, 2–50 mg/LpH 2–11Contact time, 0.5–10 h	(Xu et al., 2012)
Activated carbon	Pseudo-second-orderq_e = 43.06 mg/gk_2 = 0.0044 g/mg•min	Langmuirq_m = 91.90b = 0.64	Initial concentration, 1–160 mg/LpH 3–10Contact time, 0.5–72 h	(Martín-Lara et al., 2020)
Waste biomass-Banana bunch	Pseudo-second-orderq_e = 4.53 mg/g	Langmuir	Initial concentration, 5–100 mg/LpH 3–9Contact time, 2–38 min	(Lazim, 2021)
Porous carbon from straw waste	Pseudo-second-orderq_e = 909.10 mg/g	Langmuirk_f = 0.23 L/mg	Initial concentration, 30–300 mg/LpH 2–11Contact time, 0–480 min	(Shi et al., 2022)
Magnetic biochar	Pseudo-second orderq_e = 10.15 mg/gk_2 = 0.0155 g/mg•min	Langmuirk_l = 0.0394 L/mgq_m = 123.83 mg/g	Initial concentration, 8–200 mg/LpH 3–10Contact time, 10–180 min	(Wang and Zhang, 2020)
Bagasse-β-cyclodextrin polymer	Pseudo-second-orderq_e = 51.60 mg/gk_2 = 2.62 g/mg•min	Langmuirk_l = 0.034 L/mgq_m = 121mg/g	Initial concentration, 40–160 mg/LpH 6–9Contact time, 0–300 min	(Mpatani, 2020)
CAU-1	Pseudo-second-orderq_e = 303.03 mg/gk_2 = 0.012 g/mg•min	Freundlichk_f = 8.05 L/gn = 1.24	Initial concentration, 20–300 mg/LpH 4–10Contact time, 1–8 h	This work

Table 5 Thermodynamic parameters of BPA adsorption on CAU-1 at 25 to 80 °C.

Parameters	Temperatures (°C)			
	25.0	40.0	60.0	80.0
K_c (mg•g^{-1})•(L•mg^{-1})$^{1/n}$	0.199	0.364	0.350	0.348
ΔG (kJ•mol^{-1})	−0.493	−0.948	−0.969	−1.021
ΔH (kJ•mol^{-1})	26.722			
ΔS (J•mol^{-1}•K^{-1})	75.69			

3.6. Adsorption thermodynamics study

The thermodynamic study was conducted to explore the adsorption mechanism of BPA onto CAU-1. Table 5 shows the parameters for BPA adsorption onto CAU-1 at 25 to 80 °C. The parameters involved are Gibbs energy (ΔG), enthalpy changes (ΔH), and entropy (ΔS). ΔG was calculated using Eq. (8), while ΔH and ΔS were estimated from the graph of ln K_c against 1/T as shown using Eq. (9). A favourable condition of the thermodynamic parameters is when ΔH < 0 and ΔS > 0. When both ΔH and ΔS are at favourable conditions, the reaction is spontaneous. Therefore, the favourable ΔG is when ΔG < 0, a spontaneous reaction. ΔH is a measure of the heat content of BPA at the constant pressure of the process. The ΔH value reveals that heat was absorbed in the adsorption process, which is known as an endothermic reaction. Farias et al. reported that the chemisorption process could also be confirmed from the high value of ΔH, which can

Table 6 Comparison of thermodynamic parameters of various adsorbents.

Adsorbent	Thermodynamic constant	Thermodynamic parameter	References
Graphene	ΔG. − 10 to − 7.168 kJ•mol^{-1}ΔH. −34.383 kJ.mol^{-1}ΔS. −80.606 J.mol^{-1}. K^{-1}	Temperature, 302.15–342.15 K	(Xu et al., 2012)
Spectrogel	ΔG. − 4.5 to − 16 kJ•mol^{-1}ΔH. 79.4 kJ•mol^{-1}ΔS. 291.2 J•mol^{-1}•K^{-1}	Temperature, 15–55 °C	(de Farias et al., 2021)
CAU-1	ΔG. − 0.49 to − 1.02 kJ•mol^{-1}ΔH. 26.722 kJ•mol^{-1}ΔS. 75.69 J•mol^{-1}•K^{-1}	Temperature, 25–80 °C	This work

be observed from Table 5 (de Farias et al., 2021). The calculated enthalpy changes (ΔH) from the plotted data give a positive value (ΔH > 0), an unfavourable reaction. Thus, it is vital to examine the ΔG value to determine whether the reaction could proceed. The ΔG value becomes important when the reaction condition favours either ΔH or ΔS. The obtained ΔG values for temperatures 25, 40, 60, and 80 °C are negative (ΔG < 0), indicating that the reaction is thermodynamically viable and spontaneous. The negative value is favourable, as the reactions will convert some reactants into products, confirming that the adsorption process is chemisorption. The negative value is favourable, as the reactions will convert some reactants into products, confirming that the adsorption process is chemisorption. The ΔG value decreasing (i.e., more negative) with increasing temperature, denoting that the reaction favours at higher temperature, supported by Marrakchi et al. (Marrakchi et al., 2023). Entropy (ΔS) is the state of disorder of a system, energy to determine the molecules' dispersion or randomness in a process. The ΔS signifies the affinity of BPA to CAU-1, the tendency of BPA molecules to react with CAU-1 to form a new chemical bond through the randomness state. The obtained ΔS is positive, indicating that the adsorption of BPA into CAU-1 affects the CAU-1 structure with increasing temperature. The randomness interface of the BPA adsorption onto the CAU-1 particles intensified at higher temperature due to the higher supplied thermal energy throughout the process. A comparison of thermodynamic parameters from various works is listed in Table 6.

4. Conclusion

In this work, CAU-1 was successfully synthesised using solvothermal technique in a conventional oven. The CAU-1 characteristics were analysed using zeta potential analysis, SEM, FTIR, TGA, and XRD. SEM analysis shows that the CAU-1 crystals have a rice shape with a smooth surface and that the crystal growth follows (0 1 1) plane. The adsorption of heavy metals and BPA on CAU-1 was investigated. No significant adsorption was obtained for heavy metals. The equilibrium maximum adsorption capacity (q_m) of CAU-1 for BPA obtained from Freundlich isotherm was 303.03 mg/g at 25 °C. The kinetics and isotherm data were well fitted with pseudo-second-order model and Freundlich isotherm, respectively. The adsorption reaction was endothermic and spontaneous.

Declaration of Competing Interest

The authors declare that they have no known competing financial interests or personal relationships that could have appeared to influence the work reported in this paper.

Acknowledgement

The authors gratefully acknowledge the financial support from various parties, namely the Ministry of Higher Education under the Fundamental Research Grant Scheme (FRGS/1/2020/TK0/UTM/02/28 or R.J130000.7851.5F363), Higher Institution Centre of Excellence (HICoE) research grant (R.J090301.7851.4J422), and Universiti Teknologi Malaysia (UTM) through the Research University Grant under F4 program (Q.J130000.4646.00Q13). Appreciation also goes to UTM Research Management Centre for financial and technical support.

References

Abo El-Yazeed, W.S., Abou El-Reash, Y.G., Elatwy, L.A., Ahmed, A. I., 2020. Facile fabrication of bimetallic Fe-Mg MOF for the synthesis of xanthenes and removal of heavy metal ions. RSC Adv. 10 (16), 9693–9703. https://doi.org/10.1039/c9ra10300g.

Ahmed, M.B., Zhou, J.L., Ngo, H.H., Guo, W., Thomaidis, N.S., Xu, J., 2017. Progress in the biological and chemical treatment technologies for emerging contaminant removal from wastewater: a critical review. J. Hazard. Mater. 323, 274–298. https://doi.org/10.1016/j.jhazmat.2016.04.045.

Ahnfeldt, T. et al, 2009. Organic Framework with an Unprecedented Aluminum-Containing 4, 5163–5166. https://doi.org/10.1002/anie.200901409.

Ahnfeldt, T., Guillou, N., Gunzelmann, D., Margiolaki, I., Loiseau, T., Férey, G., Senker, J., Stock, N., 2009. [$Al_4(OH)_2(OCH_3)_4(H_2N$-bdc)$_3$]xH_2O: a 12-connected porous metal–organic framework with an unprecedented aluminum-containing brick. Angew. Chem. Int. Ed. 48 (28), 5163–5166.

Alghamdi, A.A., Al-Odayni, A.B., Saeed, W.S., Al-Kahtani, A., Alharthi, F.A., Aouak, T., 2019. Efficient adsorption of lead (II) from aqueous phase solutions using polypyrrole-based activated carbon. Materials (Basel) 12 (12). https://doi.org/10.3390/ma12122020.

Allioux, F.M. et al, 2018. Electro-capture of heavy metal ions with carbon cloth integrated microfluidic devices. Sep. Purif. Technol. 194 (August 2017), 26–32. https://doi.org/10.1016/j.seppur.2017.10.064.

Aragaw, T.A., Alene, A.N., 2022. A comparative study of acidic, basic, and reactive dyes adsorption from aqueous solution onto kaolin adsorbent: effect of operating parameters, isotherms, kinetics, and thermodynamics. Emerg. Contam. 8, 59–74. https://doi.org/10.1016/j.emcon.2022.01.002.

Boix, G. et al, 2020. MOF-Beads containing inorganic nanoparticles for the simultaneous removal of multiple heavy metals from water. ACS Appl. Mater. Interfaces 12 (9), 10554–10562. https://doi.org/10.1021/acsami.9b23206.

Chaiyasith, S., Chaiyasith, P., Septhum, C., 2006. Removal of cadmium and nickel from aqueous solution by adsorption onto treated flv ash from Thailand. Thammasat Int. J. Sc. Tech 1 (2).

Cristina, A. et al, 2019. Activated carbon produced from waste coffee grounds for an effective removal of bisphenol-A in aqueous medium. Environ. Sci. Pollut. Res., 24850–24862

de Farias, M.B., Silva, M.G.C., Vieira, M.G.A., 2021. Adsorption of bisphenol A from aqueous solution onto organoclay: experimental design, kinetic, equilibrium and thermodynamic study. Powder Technol. 395, 695–707. https://doi.org/10.1016/j.powtec.2021.10.021.

Dehghani, M.H. et al, 2016. Adsorptive removal of endocrine disrupting bisphenol A from aqueous solution using chitosan. J. Environ. Chem. Eng. 4 (3), 2647–2655. https://doi.org/10.1016/j.jece.2016.05.011.

Demirbas, A., Sari, A., Isildak, O., 2006. Adsorption thermodynamics of stearic acid onto bentonite. J. Hazard. Mater. 135 (1–3), 226–231. https://doi.org/10.1016/j.jhazmat.2005.11.056.

Deng, F., Luo, X.B., Ding, L., Luo, S.L., 2018. Application of Nanomaterials and Nanotechnology in the Reutilization of Metal Ion From Wastewater. Elsevier Inc..

Fu, F., Wang, Q., 2011. Removal of heavy metal ions from wastewaters: a review. J. Environ. Manage. 92 (3), 407–418. https://doi.org/10.1016/j.jenvman.2010.11.011.

Fuzil, N.S. et al, 2021. Bisphenol A Adsorption from Aqueous Solution Using Graphene Oxide-Alginate Beads. J. Polym. Environ. no. 0123456789. https://doi.org/10.1007/s10924-021-02226-y.

Gölzhäuser, A., 2010. Editorial: Interfacial systems chemistry: Out of the vacuum - Through the liquid - Into the cell. Phys. Chem. Chem. Phys. 12 (17), 4273–4274. https://doi.org/10.1039/c004746p.

Gonsioroski, A., Mourikes, V.E., Flaws, J.A., 2020. Endocrine disruptors in water and their effects on the reproductive system. Int. J. Mol. Sci. 21 (6). https://doi.org/10.3390/ijms21061929.

Harja, M., Buema, G., Bucur, D., 2022. Recent advances in removal of Congo Red dye by adsorption using an industrial waste. Sci. Rep., 1–18 https://doi.org/10.1038/s41598-022-10093-3.

Hashem, M.A., 2007. Adsorption of lead ions from aqueous solution by okra wastes. Int. J. Phys. Sci. 2 (7), 178–184.

Huang, L. et al, 2020. Porous and flexible membrane derived from ZIF-8-decorated hyphae for outstanding adsorption of Pb2+ ion. J. Colloid Interface Sci. 565, 465–473. https://doi.org/10.1016/j.jcis.2020.01.035.

Kim, M.K., Jo, V., Lee, D.W., Shim, I.W., Ok, K.M., 2010. CAU-1 and CAU-2: new tubular alkali metal-organic framework materials, $A_3[C_6H_3(CO_2)(CO_2H_{0.5})(CO_2H)]_2$ (A = K or Rb). CrystEngComm 12 (5), 1481–1484. https://doi.org/10.1039/b924218j.

Lalley, J., Han, C., Li, X., Dionysiou, D.D., Nadagouda, M.N., 2016. Phosphate adsorption using modified iron oxide-based sorbents in lake water: Kinetics, equilibrium, and column tests. Chem. Eng. J. 284, 1386–1396. https://doi.org/10.1016/j.cej.2015.08.114.

Lazim, Z.M. et al, 2021. Bisphenol a removal by adsorption using waste biomass: Isotherm and kinetic studies. Biointerface Res. Appl. Chem. 11 (1), 8467–8481. https://doi.org/10.33263/BRIAC111.84678481.

Li, H., Wang, F., Li, J., Deng, S., Zhang, S., 2021. Adsorption of three pesticides on polyethylene microplastics in aqueous solutions: kinetics, isotherms, thermodynamics, and molecular dynamics simulation. Chemosphere 264,. https://doi.org/10.1016/j.chemosphere.2020.128556 128556.

Marrakchi, F., Wei, M., Cao, B., Yuan, C., Chen, H., Wang, S., 2023. Copyrolysis of microalga Chlorella sp. and alkali lignin with potassium carbonate impregnation for synergistic Bisphenol A plasticizer adsorption. Int. J. Biol. Macromol. 228 (September 2022), 808–815. https://doi.org/10.1016/j.ijbiomac.2022.12.207.

Martín-Lara, M.A., Calero, M., Ronda, A., Iáñez-Rodríguez, I., Escudero, C., 2020. Adsorptive behavior of an activated carbon for bisphenol A removal in single and binary (bisphenol A-heavy metal) solutions. Water (Switzerland) 12 (8), pp. https://doi.org/10.3390/W12082150.

Mpatani, F.M. et al, 2020. Uptake of micropollutant-bisphenol A, methylene blue and neutral red onto a novel bagasse- b - cyclodextrin polymer by adsorption process. Chemosphere 259,. https://doi.org/10.1016/j.chemosphere.2020.127439 127439.

Mpatani, F.M., Han, R., Aryee, A.A., Kani, A.N., Li, Z., Qu, L., 2021. Adsorption performance of modified agricultural waste materials for removal of emerging micro-contaminant bisphenol A: a comprehensive review. Sci. Total Environ. 780,. https://doi.org/10.1016/j.scitotenv.2021.146629 146629.

Muhamad, N. et al, 2018. Removal of nickel from aqueous solution using supported zeolite-Y hollow fiber membranes. Environ. Sci. Pollut. Res. 25 (19), 19054–19064. https://doi.org/10.1007/s11356-018-2074-3.

Pauzi, M.Z.M. et al, 2019. Feasibility study of CAU-1 deposited on alumina hollow fiber for desalination applications. Sep. Purif. Technol. 217 (February), 247–257. https://doi.org/10.1016/j.seppur.2019.02.021.

Peng, Y. et al, 2018. A versatile MOF-based trap for heavy metal ion capture and dispersion. Nat. Commun. 9 (1). https://doi.org/10.1038/s41467-017-02600-2.

Petit, C., 2018. Present and future of MOF research in the field of adsorption and molecular separation. Curr. Opin. Chem. Eng. 20, 132–142. https://doi.org/10.1016/j.coche.2018.04.004.

Qasem, N.A.A., Mohammed, R.H., Lawal, D.U., 2021. Removal of heavy metal ions from wastewater: a comprehensive and critical review. npj Clean Water 4 (1), pp. https://doi.org/10.1038/s41545-021-00127-0.

Qin, Y.H., Huang, L., Zhang, D.L., Sun, L.G., 2016. Mixed-node A-Cu-BTC and porous carbon based oxides derived from A-Cu-BTC as low temperature NO-CO catalyst. Inorg. Chem. Commun. 66, 64–68. https://doi.org/10.1016/j.inoche.2016.02.005.

Rajahmundry, G.K., Garlapati, C., Kumar, P.S., Alwi, R.S., Vo, D.V.N., 2021. Statistical analysis of adsorption isotherm models and its appropriate selection. Chemosphere 276,. https://doi.org/10.1016/j.chemosphere.2021.130176 130176.

Rani, L., Kaushal, J., Srivastav, A.L., Mahajan, P., 2020. A critical review on recent developments in MOF adsorbents for the elimination of toxic heavy metals from aqueous solutions. Environ. Sci. Pollut. Res. 27 (36), 44771–44796. https://doi.org/10.1007/s11356-020-10738-8.

Shi, W., Wang, H., Yan, J., Shan, L., Quan, G., Pan, X., 2022. Wheat straw derived biochar with hierarchically porous structure for bisphenol A removal: preparation, characterization, and adsorption properties. Sep. Purif. Technol. 289, (March). https://doi.org/10.1016/j.seppur.2022.120796 120796.

Soltani, R., Pelalak, R., Pishnamazi, M., Marjani, A., Shirazian, S., 2021. A water-stable functionalized NiCo-LDH/MOF nanocomposite: green synthesis, characterization, and its environmental application for heavy metals adsorption. Arab. J. Chem. 14, (4). https://doi.org/10.1016/j.arabjc.2021.103052 103052.

Srivastava, N.K., Majumder, C.B., 2008. Novel biofiltration methods for the treatment of heavy metals from industrial wastewater. J. Hazard. Mater. 151 (1), 1–8. https://doi.org/10.1016/j.jhazmat.2007.09.101.

Sun, Z., Zhao, L., Liu, C., Zhen, Y., Ma, J., 2020. Fast adsorption of BPA with high capacity based on Π-Π electron donor-acceptor and hydrophobicity mechanism using an in-situ sp2 C dominant N-doped carbon. Chem. Eng. J. 381 (June 2019). https://doi.org/10.1016/j.cej.2019.122510.

Tsai, H.A. et al, 2006. Morphology control of polysulfone hollow fiber membranes via water vapor induced phase separation. J. Memb. Sci. 278 (1–2), 390–400. https://doi.org/10.1016/j.memsci.2005.11.029.

Van De Voorde, B., Bueken, B., Denayer, J., De Vos, D., 2014. Adsorptive separation on metal-organic frameworks in the liquid phase. Chem. Soc. Rev. 43 (16), 5766–5788. https://doi.org/10.1039/c4cs00006d.

Wang, J., Zhang, M., 2020. Adsorption characteristics and mechanism of Bisphenol A by magnetic biochar. Int. J. Environ. Res. Public Health (January 2012).

Xu, G.R., An, Z.H., Xu, K., Liu, Q., Das, R., Zhao, H.L., 2021. Metal organic framework (MOF)-based micro/nanoscaled materials for heavy metal ions removal: The cutting-edge study on designs, synthesis, and applications. Coord. Chem. Rev. 427. https://doi.org/10.1016/j.ccr.2020.213554.

Xu, J., Wang, L., Zhu, Y., 2012. Decontamination of bisphenol A from aqueous solution by graphene adsorption. Langmuir 28 (22), 8418–8425. https://doi.org/10.1021/la301476p.

Yap, P., Priyaa, V., 2019. Removal of crystal violet and acid green 25 from water using kaolin. IOP Conf Ser.: Mater. Sci. Eng. https://doi.org/10.1088/1757-899X/495/1/012052.

Yusuff, A.S., Popoola, L.T., Babatunde, E.O., 2019. Adsorption of cadmium ion from aqueous solutions by copper-based metal organic framework: equilibrium modeling and kinetic studies. Appl. Water Sci. 9 (4), 1–11. https://doi.org/10.1007/s13201-019-0991-z.

Zhao, H., Hou, S., Zhao, X., Liu, D., 2019. Adsorption and pH-responsive release of tinidazole on metal-organic framework CAU-1. J. Chem. Eng. Data 64 (4), 1851–1858. https://doi.org/10.1021/acs.jced.9b00106.

Zheng, X., Liu, S., Rehman, S., Li, Z., Zhang, P., 2020. Highly improved adsorption performance of metal-organic frameworks CAU-1 for trace toluene in humid air via sequential internal and external surface modification. Chem. Eng. J. 389 (October 2019), 123424. https://doi.org/10.1016/j.cej.2019.123424.

Zheng, X., Liu, S., Rehman, S., Li, Z., Zhang, P., 2020. Highly improved adsorption performance of metal-organic frameworks CAU-1 for trace toluene in humid air via sequential internal and external surface modification. Chem. Eng. J. 389 (August 2019). https://doi.org/10.1016/j.cej.2019.123424.

Zhong, X., Liang, W., Wang, H., Xue, C., Hu, B., 2021. Aluminum-based metal-organic frameworks (CAU-1) highly efficient UO_2^{2+} and TcO_4^- ions immobilization from aqueous solution. J. Hazard. Mater. 407 (December 2020). https://doi.org/10.1016/j.jhazmat.2020.124729.